Editors' Suggestion

Unitary control of multiport wave transmission

Cheng Guo,* David A. B. Miller, and Shanhui Fan†
Ginzton Laboratory and Department of Electrical Engineering, Stanford University, Stanford, California 94305, USA

(Received 9 August 2024; accepted 17 January 2025; published 10 February 2025)

Controlling wave transmission is crucial for various applications. In this work we apply the concept of unitary control to manipulate multiport wave transmission. Unitary control aims to control the behaviors of a set of orthogonal waves simultaneously. The approach fully harnesses the capability of wavefront shaping techniques, with promising applications in communication, imaging, and photonic integrated circuits. Here we present a detailed theory of unitary control of wave transmission, focusing on two key characteristics: total (power) transmittance and direct (field) transmission. The total transmittance for an input port represents the fraction of total transmitted power with respect to the input power for a wave incident from an input port. The direct transmission for an input port denotes the complex transmission amplitude from that input port to its corresponding output port. We address two main questions: (i) the achievable total transmittance and direct transmission for each port and (ii) the configuration of unitary control to attain desired transmission values for each port. Our theory illustrates that unitary control enables uniform total transmittance and direct transmission across any medium. Furthermore, we show that reciprocity and energy conservation enforce direct symmetry constraints on wave transmission in both the forward and backward directions under unitary control.

DOI: 10.1103/PhysRevA.111.023507

I. INTRODUCTION

Controlling the transmission of waves through complex media is crucial for various applications in imaging [1–12], communications [13–15], sensing [16–20], photonic integrated circuits [21–23], and spatiotemporal wave shaping [24–26]. Recent advancements [27–32] have allowed for precise control over coherent wave transport in complex media [33,34] including highly scattering biological tissues [2,29,31,35] and multimode optical fibers [3,36–40], enabling applications such as spatial and temporal focusing [19,29,38,41–47], transmittance enhancement and suppression [16,48–58], and optical micromanipulation [59–61].

A key development in wave transmission control has been the use of wavefront shaping techniques, particularly spatial light modulators (SLMs) [62,63]. Spatial light modulators can adjust the phase of reflected light to tailor a coherent input field into a customized wavefront, resulting in the desired transmitted pattern after passing through the complex medium. This process, known as coherent control [18,55,64,65], has revolutionized our ability to control wave propagation through complex media.

However, initial works on coherent control through SLMs have been primarily limited to a single incident wave, while many applications require the simultaneous control of multiple orthogonal waves [66–68]. This multiport control is becoming possible with programmable unitary photonic devices like Mach-Zehnder interferometer (MZI) meshes [13,69–81] and multiplane light conversion devices [82–87]. These devices can perform arbitrary unitary transformations and hold promise for various applications in quantum computing [72,88–93], machine learning [94–101], and optical communications [74,77,102–105]. By transforming from one set of orthogonal incident waves to another, they can achieve sophisticated multiport transmission control. We refer to such control as unitary control [106–109], as it is mathematically represented by a unitary transformation of the input wave space. References [13,15] show explicit physical examples of such unitary control.

In this paper we present a systematic theory of unitary control over multiport wave transmission. Some optimum results are already known from the singular-value decomposition (SVD) approach to waves and optics [110,111]. Such SVD optimum orthogonal channels between inputs and outputs, which can be thought of as communication modes [14,110] or mode-converter basis sets [14,111], can be found and implemented physically using unitary control from MZI meshes [13–15]. Beyond these SVD modes, other sets of orthogonal waves are relevant in various contexts. For instance, principal modes in multimode waveguides exhibit minimal modal dispersion and form orthogonal bases at both waveguide ends [36]. Additionally, orbital angular momentum modes are common in multimode fiber communications [112–116]. Understanding the transmission properties of these diverse orthogonal wave sets is thus valuable.

When analyzing the transmission properties of orthogonal waves, several key characteristics are essential for each input wave basis: total transmittance, direct transmission, and crosstalk. These quantities are defined after selecting orthogonal bases at both input and output ends of the medium, e.g., a waveguide. For an incident wave in the ith input port, the total transmittance T_i represents the fraction of power transmitted

*Contact author: guocheng@stanford.edu
†Contact author: shanhui@stanford.edu

with respect to the input power. The direct transmission t_i denotes the complex transmission amplitude to the ith output port. Crosstalk, calculated as $T_i - |t_i|^2$, describes the fraction of power transmitted to output ports other than the ith output port. Though a full transmission matrix is required to describe the transmission properties of the medium, the total transmission and the crosstalk usefully characterize the power transmission properties of the ith input basis wave through the medium.

Here we address two fundamental questions for the transmission of orthogonal waves in unitary control. (i) What are the possible values of total transmittance and direct transmission for each input port under unitary control in a given medium? (ii) How can we configure unitary control to achieve specific total transmittance or direct transmission for each port? We answer these questions using matrix inequalities. Our results provide insights into the principles and implementations of the unitary control method.

The rest of this paper is organized as follows. In Sec. II we summarize the useful mathematical notation. In Sec. III we develop a general theory of unitary control over wave transmission. In Sec. IV we discuss the physical applications of our theory. In Sec. V we provide a numerical illustration of our theory. We summarize in Sec. VI. The Appendices contain additional information. Appendices A–C provide details and demonstrations of the algorithms. Appendix D provides detailed mathematical proof.

II. NOTATION

We first summarize the notation related to matrices. We denote by M_n the set of $n \times n$ complex matrices and $\mathrm{U}(n)$ the set of $n \times n$ unitary matrices. For $M \in M_n$, we define $\boldsymbol{d}(M) = (d_1(M), \ldots, d_n(M))^{\mathrm{T}}$, $\boldsymbol{\lambda}(M) = (\lambda_1(M), \ldots, \lambda_n(M))^{\mathrm{T}}$, and $\boldsymbol{\sigma}(M) = (\sigma_1(M), \ldots, \sigma_n(M))^{\mathrm{T}}$ as the vectors of diagonal entries, eigenvalues, and singular values of M [117]. We also define

$$\boldsymbol{\sigma}^2(M) \equiv \left(\sigma_1^2(M), \ldots, \sigma_n^2(M)\right)^{\mathrm{T}}. \tag{1}$$

(We take the convention of choosing the singular values to be real numbers, with any complex phase factors instead included in the corresponding singular functions.) Finally, for $\boldsymbol{z} = (z_1, \ldots, z_n)^{\mathrm{T}} \in \mathbb{C}^n$, we define $|\boldsymbol{z}| = (|z_1|, \ldots, |z_n|)^{\mathrm{T}} \in \mathbb{R}^n$. (The superscript T here means the transpose, giving a more compact way of writing a column vector.)

We also discuss the notation of majorization [118]. For $\boldsymbol{x} = (x_1, x_2, \ldots, x_n) \in \mathbb{R}^n$, we define $\boldsymbol{x}^{\downarrow} = (x_1^{\downarrow}, x_2^{\downarrow}, \ldots, x_n^{\downarrow})$, where $x_1^{\downarrow} \geqslant x_2^{\downarrow} \geqslant \cdots \geqslant x_n^{\downarrow}$, hence reordering the components of x in nonincreasing order. For $\boldsymbol{x} = (x_1, \ldots, x_n)$ and $\boldsymbol{y} = (y_1, \ldots, y_n)$ in $\mathbb{R}^n$, if

$$\sum_{i=1}^{k} x_i^{\downarrow} \leqslant \sum_{i=1}^{k} y_i^{\downarrow}, \quad k = 1, 2, \ldots, n-1 \tag{2}$$

$$\sum_{i=1}^{n} x_i = \sum_{i=1}^{n} y_i, \tag{3}$$

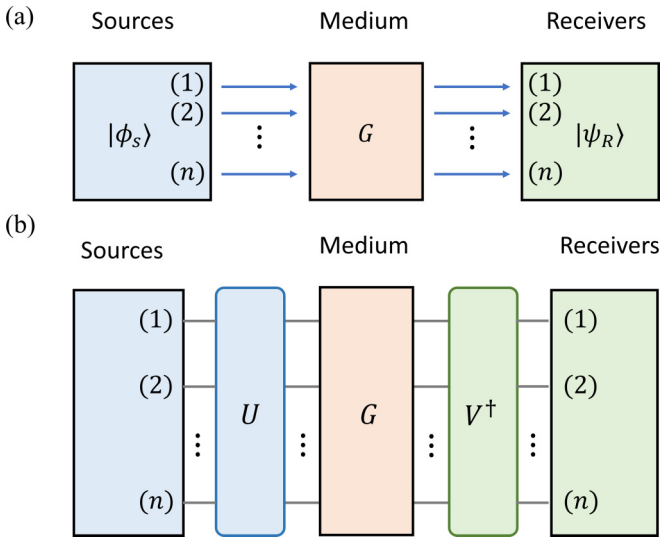

FIG. 1. (a) Scheme of wave transmission. An input wave $|\phi_S\rangle$ passes through the medium and becomes the transmitted wave $|\psi_R\rangle = G|\phi_S\rangle$. (b) Unitary control of wave transmission. Input ports and output ports are numbered from (1) to (n).

we say that $\boldsymbol{x}$ is majorized by $\boldsymbol{y}$, written as $\boldsymbol{x} \prec \boldsymbol{y}$. If Eq. (3) is replaced by a corresponding inequality

$$\sum_{i=1}^{n} x_i \leqslant \sum_{i=1}^{n} y_i, \tag{4}$$

we say that $\boldsymbol{x}$ is weakly majorized by $\boldsymbol{y}$, written as $\boldsymbol{x} \prec_w \boldsymbol{y}$.

III. THEORY

A. Wave transmission

Consider a typical setup for wave transmission, where waves are emitted from multiple sources, transmitted through a medium, and detected by several receivers [14] [see Fig. 1(a)]. The medium is assumed to be a linear time-invariant system with two sides, each having n ports. We consider a set of input ports, with the wave in the jth input port being written as $|\phi_j^{(i)}\rangle$ and the wave in the jth output port being written as $|\psi_j^{(o)}\rangle$. The wave in one input (or output) port by definition does not overlap with the wave in any other input (or output) port, so this port by port set of input functions is orthogonal, and similarly for the corresponding port by port set of output functions. Using these port functions as bases, we can describe the input and transmitted waves as the vectors of amplitudes

$$\boldsymbol{a} = (a_1, \ldots, a_n)^{\mathrm{T}}, \quad \boldsymbol{b} = (b_1, \ldots, b_n)^{\mathrm{T}}, \tag{5}$$

where a_i and b_i represent the input and transmitted wave amplitudes in their respective ports. The transmission process is described by a complex transmission matrix $G \in M_n$ (which can also be considered as a coupling matrix, a device matrix, or a Green's function matrix) [14,48,49,119],

$$\boldsymbol{b} = G\boldsymbol{a}, \tag{6}$$

where G_{ij} represents the transmission coefficient from the jth port on the left to the ith port on the right.

B. Unitary control of wave transmission

Now we introduce unitary control. Unitary control refers to unitarily transforming the input and transmitted wave bases [Fig. 1(b)]

$$|\phi_j^{(i)}\rangle \to |\phi_j^{(i)}[U]\rangle = \sum_{k=1}^{n} U_{kj}|\phi_k^{(i)}\rangle,$$
$$|\psi_j^{(o)}\rangle \to |\psi_j^{(o)}[V]\rangle = \sum_{k=1}^{n} V_{kj}|\psi_k^{(o)}\rangle, \tag{7}$$

where $U, V \in \mathrm{U}(n)$. Throughout the paper, we use square brackets to indicate the dependence on a matrix. The resulting transformed basis functions are themselves now n-dimensional vectors of amplitudes. Because unitary operations preserve orthogonality, these new bases are also orthogonal. Under the new bases, the transmission matrix is modified to

$$G \to G[U, V] = V^\dagger G U. \tag{8}$$

Hence, unitary control corresponds to a unitary equivalence [120] of a transmission matrix.

Unitary control also transforms the transmission properties of a system. We focus on two key characteristics: total (power) transmittance and direct (field) transmission. The total transmittance [55] is described by a real total transmittance vector

$$\boldsymbol{T} := (T_1, \ldots, T_n)^{\mathrm{T}}, \tag{9}$$

where $T_i \in \mathbb{R}$ represents the total power transmitted when a wave with unit power is incident from the ith input port only. The direct transmission is described by a complex direct transmission vector

$$\boldsymbol{t} := (t_1, t_2, \ldots, t_n)^{\mathrm{T}}, \tag{10}$$

where $t_i \in \mathbb{C}$ represents the amplitude transmission coefficient from the ith input port to the ith transmitted port. These input and transmitted ports can be chosen freely, but in many practical scenarios, there is a natural choice. For example, in a multimode fiber, the orbital angular momentum (OAM) modes are often chosen as input and transmitted bases [112–116]. Then the direct transmission describes the transmission coefficients between the same OAM modes. Because the OAM modes are transmitted without mixing in such an ideal fiber, $\boldsymbol{T}$ just becomes the vector of power transmissions of these modes and $\boldsymbol{t}$ just becomes the vector of the amplitude transmissions of these modes. Then G and $G^\dagger G$ become diagonal matrices in this basis so that, formally, in our notation

$$\boldsymbol{T} = \boldsymbol{d}(G^\dagger G), \quad \boldsymbol{t} = \boldsymbol{d}(G). \tag{11}$$

Under the unitary control as defined in Eq. (8), the total transmittance vector in the new bases is modified to

$$\boldsymbol{T} \to \boldsymbol{T}[U] := \boldsymbol{d}(G^\dagger[U, V] G[U, V]) = \boldsymbol{d}(U^\dagger G^\dagger G U), \tag{12}$$

which depends only on U. Similarly, the direct transmission vector in the new bases is modified to

$$\boldsymbol{t} \to \boldsymbol{t}[U, V] := \boldsymbol{d}(G[U, V]) = \boldsymbol{d}(V^\dagger G U), \tag{13}$$

which depends on both U and V.

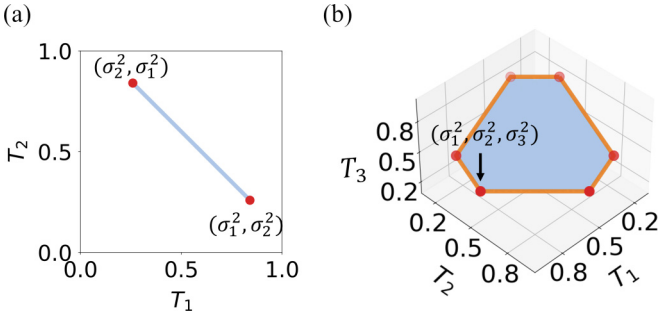

FIG. 2. Examples of $\{\boldsymbol{T}\}$ for (a) $G_2 \in M_2$ with $\boldsymbol{\sigma}^2(G_2) = (0.84, 0.26)^{\mathrm{T}}$ and (b) $G_3 \in M_3$ with $\boldsymbol{\sigma}^2(G_3) = (0.81, 0.36, 0.16)^{\mathrm{T}}$.

C. Major questions

We ask four basic questions: Given a transmission medium under unitary control, (1) what total transmittance vectors are attainable, (2) how is a given total transmittance vector obtained, (3) what direct transmission vectors are attainable, and (4) how is a given direct transmission vector obtained? Questions 1 and 3 ask about the capability and limitation of unitary control. Questions 2 and 4 ask for implementation.

We now reformulate these key questions mathematically. Let $G \in M_n$ be a given transmission matrix.

Question 1. What is the set

$$\{\boldsymbol{T}\} := \{\boldsymbol{T}[U] \mid U \in \mathrm{U}(n)\}? \tag{14}$$

Question 2 Given $\boldsymbol{T}_0 \in \{\boldsymbol{T}\}$, what is the set

$$\{U[\boldsymbol{T}_0]\} := \{U \in \mathrm{U}(n) \mid \boldsymbol{T}[U] = \boldsymbol{T}_0\}? \tag{15}$$

Question 3. What is the set

$$\{\boldsymbol{t}\} := \{\boldsymbol{t}[U, V] \mid U, V \in \mathrm{U}(n)\}? \tag{16}$$

Question 4. Given $\boldsymbol{t}_0 \in \{\boldsymbol{t}\}$, what is the set

$$\{(U, V)[\boldsymbol{t}_0]\} := \{U, V \in \mathrm{U}(n) \mid \boldsymbol{t}[U, V] = \boldsymbol{t}_0\}? \tag{17}$$

D. Main results

Here we provide complete answers to Questions 1–3 and a partial answer to Question 4.

1. Answer to Question 1

We start with Question 1. To hint at the solution, we perform two numerical experiments. In the first experiment, we consider a random 2×2 transmission matrix

$$G_2 = \begin{pmatrix} 0.4 - 0.5i & 0.1 + 0.3i \\ 0.4 - 0.3i & 0.5 - 0.3i \end{pmatrix}, \tag{18}$$

$$\boldsymbol{\sigma}(G_2) = \begin{pmatrix} 0.92 \\ 0.51 \end{pmatrix}, \quad \boldsymbol{\sigma}^2(G_2) = \begin{pmatrix} 0.84 \\ 0.26 \end{pmatrix}. \tag{19}$$

We generate 1000 random $U_i \in \mathrm{U}(2)$ and calculate $\boldsymbol{T}[U_i]$ by Eq. (12). Figure 2(a) shows the result. We see that $\{\boldsymbol{T}\}$ is a line segment with endpoints obtained by permuting the coordinates of $\boldsymbol{\sigma}^2(G_2)$. In the second experiment, we consider a

random 3×3 scattering matrix

$$G_3 = \begin{pmatrix} -0.14 - 0.07i & -0.19 - 0.27i & 0.55 - 0.04i \\ -0.48 - 0.26i & -0.09 - 0.12i & -0.23 - 0.38i \\ -0.02 - 0.03i & 0.22 - 0.44i & -0.14 - 0.34i \end{pmatrix}, \tag{20}$$

$$\boldsymbol{\sigma}(G_3) = \begin{pmatrix} 0.90 \\ 0.60 \\ 0.40 \end{pmatrix}, \quad \boldsymbol{\sigma}^2(G_3) = \begin{pmatrix} 0.81 \\ 0.36 \\ 0.16 \end{pmatrix}. \tag{21}$$

We generate 100000 random $U_i \in \mathrm{U}(3)$ and calculate $\boldsymbol{T}[U_i]$ by Eq. (12). Figure 2(b) shows the result. We see that $\{\boldsymbol{T}\}$ is a convex hexagon with vertices obtained by permuting the coordinates of $\boldsymbol{\sigma}^2(G_3)$.

The numerical results above suggest the following observation on the geometry of $\{\boldsymbol{T}\}$: For an $n \times n$ transmission matrix G, $\{\boldsymbol{T}\}$ is a convex subset of an $(n-1)$-dimensional hyperplane in $\mathbb{R}^n$. It is the convex hull spanned by the $n!$ points obtained by permuting the coordinates of $\boldsymbol{\sigma}^2(G)$. [We note that the convex hull of a set is the smallest convex set that contains it, and $\boldsymbol{\sigma}^2(G) = \boldsymbol{\lambda}(G^\dagger G)$ is also known as the transmission eigenvalues [121].] We show that this observation is true as a result of our first theorem.

Theorem 1. Given a transmission matrix $G \in M_n$,

$$\{\boldsymbol{T}\} = \{\boldsymbol{u} \in \mathbb{R}^n | \boldsymbol{u} \prec \boldsymbol{\sigma}^2(G)\}. \tag{22}$$

Proof. First, we show $\boldsymbol{T}[U] \in \{\boldsymbol{T}\} \Rightarrow \boldsymbol{T}[U] \prec \boldsymbol{\sigma}^2(G)$. We use Schur's theorem [122]

$$\boldsymbol{T}[U] = \boldsymbol{d}(U^\dagger G^\dagger G U) \prec \boldsymbol{\lambda}(U^\dagger G^\dagger G U) = \boldsymbol{\lambda}(G^\dagger G) = \boldsymbol{\sigma}^2(G). \tag{23}$$

Second, we show $\boldsymbol{u} \prec \boldsymbol{\sigma}^2(G) \Rightarrow \boldsymbol{u} \in \{\boldsymbol{T}\}$, i.e., there exists $U \in \mathrm{U}(n)$ such that $\boldsymbol{T}[U] = \boldsymbol{u}$. We use Horn's theorem [123]: As $\boldsymbol{u} \prec \boldsymbol{\sigma}^2(G)$, there exists a Hermitian matrix H with $\boldsymbol{d}(H) = \boldsymbol{u}$ and $\boldsymbol{\lambda}(H) = \boldsymbol{\sigma}^2(G)$. Since $\lambda(G^\dagger G) = \boldsymbol{\sigma}^2(G) = \lambda(H)$, H and $G^\dagger G$ are unitarily similar. Hence there exists $U \in \mathrm{U}(n)$ such that $H = U^\dagger G^\dagger G U$. Now we check

$$\boldsymbol{T}[U] \equiv \boldsymbol{d}(U^\dagger G^\dagger G U) = \boldsymbol{d}(H) = \boldsymbol{u}. \tag{24}$$

This completes the proof. ■

The geometric observation above is a direct consequence of Theorem 1. We use Rado's theorem [124], which states that for a given $\boldsymbol{y} \in \mathbb{R}^n$, the set $\{\boldsymbol{x} \in \mathbb{R}^n | \boldsymbol{x} \prec \boldsymbol{y}\}$ is the convex hull of points obtained by permuting the components of $\boldsymbol{y}$. The geometric observation is an application of Rado's theorem to Eq. (22).

It should be noted that the necessary condition $\boldsymbol{T}[U] \in \boldsymbol{T} \Rightarrow \boldsymbol{T}[U] \prec \boldsymbol{\sigma}^2(G)$ is known in the literature in some equivalent form [14,110] but not proven using majorization theory. This implies that no channels can outperform SVD channels [14]. The sufficient condition, stating that for any $\boldsymbol{u} \prec \boldsymbol{\sigma}^2(G)$ there exists $U \in \mathrm{U}(n)$ such that $\boldsymbol{T}[U] = \boldsymbol{u}$, is a new result. It demonstrates that any power distribution channels not superior to SVD channels in the majorization sense can be achieved through unitary control.

Equation (22) is our first main result. It shows that $\{\boldsymbol{T}\}$ is completely determined by $\boldsymbol{\sigma}(G)$, which is invariant under unitary control: $\boldsymbol{\sigma}(V^\dagger G U) = \boldsymbol{\sigma}(G)$. We can classify all transmission media by their $\boldsymbol{\sigma}$. Two media exhibit the same $\{\boldsymbol{T}\}$ if and only if they belong to the same $\boldsymbol{\sigma}$ class.

2. Answer to Question 2

Now we turn to Question 2. The problem corresponds to the following physical scenario. Suppose we have a medium characterized by a transmission matrix G. Given a total transmittance vector $\boldsymbol{T}_0 \prec \boldsymbol{\sigma}^2(G)$, how do we construct the set of all possible unitary control schemes as described by unitary matrices $\{U[\boldsymbol{T}_0]\}$ that achieve $\boldsymbol{T}_0$? Alternatively, a simpler question is how to construct one unitary control scheme as described by a unitary matrix $U[\boldsymbol{T}_0]$ that achieves $\boldsymbol{T}_0$.

These two problems can be solved by the following algorithms. We first perform a preparatory step that is common in both algorithms. Suppose G has p distinct singular values. Then $G^\dagger G$ has p distinct eigenvalues $\lambda_1, \ldots, \lambda_p$, with respective multiplicities $n_1, \ldots, n_p$. Let $\Lambda = \lambda_1 I_{n_1} \oplus \ldots \oplus \lambda_p I_{n_p}$. We find a $V \in \mathrm{U}(n)$ such that $G^\dagger G = V \Lambda V^\dagger$. Now we provide the two algorithms.

ALGORITHM 1. Constructing $\{U[\boldsymbol{T}_0]\}$.

(i) Use Fickus's algorithm [125] (see Appendix A for details) to construct all Hermitian matrices H_i with eigenvalues $\boldsymbol{\lambda}(G^\dagger G)$ and diagonal entries $\boldsymbol{T}_0$. For each H_i, find a $V_i \in \mathrm{U}(n)$ such that $H_i = V_i \Lambda V_i^\dagger$.
(ii) We claim that $U_i \in \mathrm{U}(n)$ such that $H_i = U_i^\dagger G^\dagger G U_i$ if and only if

$$U_i = V(W_1 \oplus \cdots \oplus W_p) V_i^\dagger, \tag{25}$$

where $W_k \in \mathrm{U}(n_k)$, $k = 1, \ldots, p$, are arbitrary. Denote the set of all such U_i by $\{U_i\}$.
(iii) We claim that $\{U[\boldsymbol{T}_0]\} = \bigcup_i \{U_i\}$. (See the Supplemental Material of Ref. [106] for proof of the two claims.)

ALGORITHM 2. Constructing a $U[\boldsymbol{T}_0]$.

(i) Use Chu's first algorithm [126] (see Appendix A for details) to construct a Hermitian matrix H with eigenvalues $\boldsymbol{\lambda}(G^\dagger G)$ and diagonal elements $\boldsymbol{T}_0$. Find a $V' \in \mathrm{U}(n)$ such that $H = V' \Lambda V'^\dagger$.
(ii) We obtain a $U[\boldsymbol{T}_0] = V V'^\dagger$.

Algorithms 1 and 2 are our second main result. We illustrate their usage with a numerical example in Appendix B. We consider a 5×5 transmission matrix G. Our task is to construct a $U[\boldsymbol{T}_0]$ with a randomly assigned goal $\boldsymbol{T}_0$. We use Algorithm 2 and complete the task. Importantly, our algorithms allow us to achieve the prescribed total transmittance in all ports with a single unitary matrix that performs the unitary control.

3. Answer to Question 3

Next we consider Question 3. To hint at the solution, we perform two numerical experiments. In the first experiment, we consider the 2×2 transmission matrix G_2 in Eq. (18). We generate 1000000 random $(U_i, V_i) \in \mathrm{U}(2) \times \mathrm{U}(2)$ and calculate $\boldsymbol{t}[U_i, V_i]$ by Eq. (13). Figure 3(a) shows the

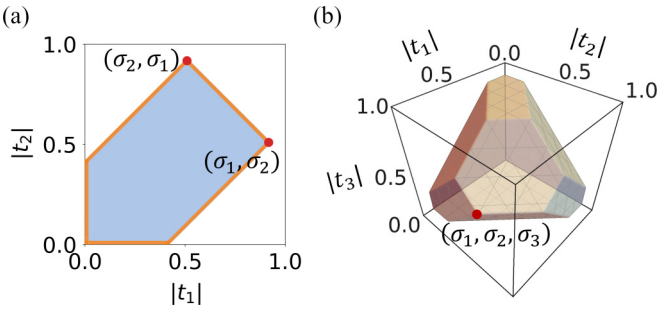

FIG. 3. Examples of $\{|\boldsymbol{t}|\}$ for (a) $G_2 \in M_2$ with $\boldsymbol{\sigma}(G_2) = (0.92, 0.51)^{\mathrm{T}}$ and (b) $G_3 \in M_3$ with $\boldsymbol{\sigma}(G_3) = (0.90, 0.60, 0.40)^{\mathrm{T}}$.

result of $|\boldsymbol{t}|[U_i, V_i]$.[1] We see that $\{|\boldsymbol{t}|\}$ is a convex pentagon, which is defined by the set of solutions to a system of linear inequalities[2]

$$|t|_1^{\downarrow} \leqslant \sigma_1^{\downarrow}(G_2), \tag{26}$$

$$|t|_1^{\downarrow} + |t|_2^{\downarrow} \leqslant \sigma_1^{\downarrow}(G_2) + \sigma_2^{\downarrow}(G_2), \tag{27}$$

$$|t|_1^{\downarrow} - |t|_2^{\downarrow} \leqslant \sigma_1^{\downarrow}(G_2) - \sigma_2^{\downarrow}(G_2). \tag{28}$$

In the second experiment, we consider the 3×3 transmission matrix G_3 in Eq. (20). We generate 10000000 random $(U_i, V_i) \in \mathrm{U}(3) \times \mathrm{U}(3)$ and calculate $\boldsymbol{t}[U_i, V_i]$ by Eq. (13). Figure 3(a) shows the result of $|\boldsymbol{t}|[U_i, V_i]$. We see that $\{|\boldsymbol{t}|\}$ is a convex decahedron, which is defined by the set of solutions to a system of linear inequalities[3]

$$|t|_1^{\downarrow} \leqslant \sigma_1^{\downarrow}(G_3), \tag{29}$$

$$|t|_1^{\downarrow} + |t|_2^{\downarrow} \leqslant \sigma_1^{\downarrow}(G_3) + \sigma_2^{\downarrow}(G_3), \tag{30}$$

$$|t|_1^{\downarrow} + |t|_2^{\downarrow} + |t|_3^{\downarrow} \leqslant \sigma_1^{\downarrow}(G_3) + \sigma_2^{\downarrow}(G_3) + \sigma_3^{\downarrow}(G_3), \tag{31}$$

$$|t|_1^{\downarrow} + |t|_2^{\downarrow} - |t|_3^{\downarrow} \leqslant \sigma_1^{\downarrow}(G_3) + \sigma_2^{\downarrow}(G_3) - \sigma_3^{\downarrow}(G_3). \tag{32}$$

The numerical results above suggest the following observation on the geometry of $\{|\boldsymbol{t}|\}$: For an $n \times n$ transmission matrix G, $\{|\boldsymbol{t}|\}$ is a convex polytope in $\mathbb{R}^n$, bounded by an intersection of half planes. The half planes are defined by a set of linear inequalities involving the coordinates of $\boldsymbol{\sigma}(G)$. We show that this observation is true as a result of our second theorem.

Theorem 2. Given a transmission matrix $G \in M_n$,

$$\{\boldsymbol{t}\} = \Bigg\{ \boldsymbol{v} \in \mathbb{C}^n \mid |\boldsymbol{v}| \prec_w \boldsymbol{\sigma}(G), \sum_{i=1}^{n-1} |\boldsymbol{v}|_i^{\downarrow} - |\boldsymbol{v}|_n^{\downarrow} \leqslant \sum_{i=1}^{n-1} \boldsymbol{\sigma}_i^{\downarrow}(G) - \boldsymbol{\sigma}_n^{\downarrow}(G) \Bigg\}. \tag{33}$$

Proof. This can be proved using the Sing-Thompson theorem [127–129]. ■

[1] It is easy to see that the phases of $\boldsymbol{t}$ components can be arbitrary when one considers all possible (U_i, V_i).

[2] Inequality (26) is redundant but included for later generalization.

[3] Inequality (30) is redundant but included for later generalization.

Equation (33) is our third main result. It shows that $\{\boldsymbol{t}\}$ is completely determined by $\boldsymbol{\sigma}(G)$. Two media exhibit the same $\{\boldsymbol{t}\}$ if and only if they belong to the same $\boldsymbol{\sigma}$ class. We also note that only the magnitudes of t_i are constrained by Eq. (33), while the phases of t_i can be arbitrarily set, e.g., by considering a diagonal unitary transformation U or V.

4. Answer to Question 4

Finally, we discuss Question 4. The problem corresponds to the following physical scenario. Suppose we have a medium characterized by a transmission matrix G. Given a direct transmission vector $\boldsymbol{t}_0 \in \{\boldsymbol{t}\}$, how do we construct the set of all possible unitary control schemes as described by unitary matrix pairs $\{(U, V)[\boldsymbol{t}_0]\}$ that achieve $\boldsymbol{t}_0$? Alternatively, a simpler question is how to construct one unitary control scheme as described by a unitary matrix pair $(U, V)[\boldsymbol{t}_0]$ that achieves $\boldsymbol{t}_0$.

We do not have the answer to the first problem yet. We provide an algorithm that solves the second problem.

ALGORITHM 3. Constructing a $(U, V)[\boldsymbol{t}_0]$.

(i) Calculate the SVD of G: $G = V_0^{\dagger} \Sigma U_0$.
(ii) Use Chu's second algorithm [130] (see Appendix A for details) to construct a complex matrix G' with singular values $\boldsymbol{\sigma}(G)$ and diagonal elements $\boldsymbol{t}_0$. Calculate the SVD of G': $G' = V'^{\dagger} \Sigma U'$.
(iii) We obtain a $(U, V)[\boldsymbol{t}_0] = (U_0^{\dagger} U', V_0^{\dagger} V')$.

Algorithm 3 is our fourth main result. We illustrate its usage with a numerical example in Appendix C. We consider a 5×5 transmission matrix G. Our task is to construct a $(U, V)[\boldsymbol{T}_0]$ with a randomly assigned goal $\boldsymbol{t}_0$. We use Algorithm 3 and complete the task. Importantly, our algorithm allows us to achieve the prescribed direct transmission in all ports with a single unitary matrix pair that performs the unitary control.

IV. APPLICATIONS

Now we discuss the physical applications of our theory.

A. Multimode coherent perfect or zero transmission

First, we provide the criterion for k-fold degenerate coherent perfect transmittance, i.e., the effect that a medium exhibits perfect total transmittance for k independent coherent input waves. From Eq. (22) we obtain a necessary and sufficient condition for $G \in M_n$:

$$\boldsymbol{\sigma}_1^{\downarrow}(G) = \cdots = \boldsymbol{\sigma}_k^{\downarrow}(G) = 1. \tag{34}$$

Similarly, we provide the criterion for k-fold degenerate coherent zero transmittance, i.e., the effect that a medium exhibits zero total transmittance for k independent coherent input waves. From Eq. (22) we obtain a necessary and sufficient condition for $G \in M_n$:

$$\boldsymbol{\sigma}_1^{\downarrow}(G) = \cdots = \boldsymbol{\sigma}_k^{\downarrow}(G) = 0. \tag{35}$$

B. Unitary uniform transmission

Second, we propose the concepts of unitary uniform total transmittance and unitary uniform direct transmission, which refer to the effects that a medium exhibits uniform total transmittance ($T_i = \text{const}$) and uniform direct transmission ($t_i = \text{const}$), respectively, under some unitary control. We claim that any medium exhibits unitary uniform total transmittance. We prove this by showing that for any $G \in M_n$, there exist $U \in \mathrm{U}(n)$ such that

$$\boldsymbol{T}[U] = (a, \ldots, a)^{\mathrm{T}}, \quad a = \frac{1}{n}\sum_{i=1}^{n} \sigma_i^2(G). \tag{36}$$

This is because for any $(x_1, x_2, \ldots, x_n)^{\mathrm{T}} \in \mathbb{R}^n$, we have

$$(\bar{x}, \bar{x}, \ldots, \bar{x})^{\mathrm{T}} \prec (x_1, x_2, \ldots, x_n)^{\mathrm{T}}, \quad \bar{x} = \frac{1}{n}\sum_{i=1}^{n} x_i. \tag{37}$$

Thus, for any $G \in M_n$, we have

$$(a, \ldots, a)^{\mathrm{T}} \prec \boldsymbol{\sigma}^2(G); \tag{38}$$

hence by Eq. (22), it is attainable under unitary control. Moreover, we claim that any medium exhibits unitary uniform direct transmission. We prove this by showing that for any $G \in M_n$ and for any $b \in \mathbb{C}$ that satisfies

$$|b| \leqslant \frac{1}{n}\sum_{i=1}^{n} \sigma_i(G), \tag{39}$$

there exist $(U, V) \in \mathrm{U}(n) \times \mathrm{U}(n)$ such that

$$\boldsymbol{t}[U, V] = (b, \ldots, b)^{\mathrm{T}}. \tag{40}$$

This is because $(b, \ldots, b)^{\mathrm{T}}$ satisfies all the inequalities in Eq. (33); hence it is attainable under unitary control. So any transmission medium can exhibit uniform total transmittance or direct transmission over any number of ports under suitable unitary control. Moreover, our algorithms provide practical implementations to achieve these effects. These results can be useful in applications such as uniform illumination.

C. Symmetry constraints on bilateral transmission

Third, we discuss the constraints imposed by symmetry on the unitary control of bilateral transmission. So far, our focus has been on the transmission matrix G in the forward direction (from left to right). However, in many applications, it is also necessary to consider the transmission matrix $\tilde{G}$ in the backward direction (from right to left). In general, G and $\tilde{G}$ can be distinct. Nevertheless, certain symmetries of the system can establish a relationship between them, thereby affecting their unitary control. Here we examine two significant internal symmetries [131,132]: reciprocity and energy conservation. We have proven that when the medium is either reciprocal or energy conserving,

$$\boldsymbol{\sigma}(\tilde{G}) = \boldsymbol{\sigma}(G). \tag{41}$$

(See Appendix D for proof.) Consequently, G and $\tilde{G}$ belong to the same $\boldsymbol{\sigma}$ class and exhibit the same sets of attainable $\{\boldsymbol{T}\}$ and $\{\boldsymbol{t}\}$ under unitary control.

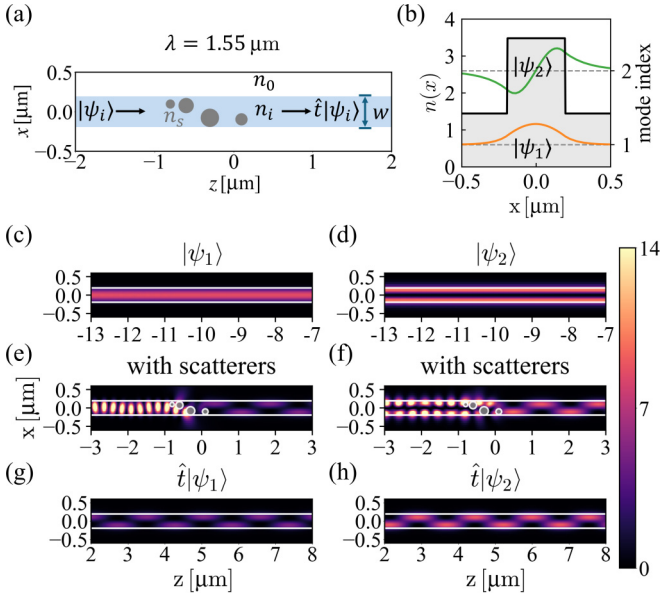

FIG. 4. Silicon slab waveguide with embedded scatterers. (a) The waveguide structure consists of a silicon core ($n_i = 3.48$) embedded in silica ($n_0 = 1.444$) with four cylindrical scatterers made of lossy silica ($n_s = 1.444 + 0.100i$). The geometric parameters are provided in the text. The uniform waveguide section supports two eigenmodes $|\psi_1\rangle$ and $|\psi_2\rangle$. (b) Refractive index profile $n(x)$ (left axis) and eigenmode electric field distributions for $|\psi_1\rangle$ and $|\psi_2\rangle$ (right axis). Intensity distributions $|E|^2(x, z)$ show the input eigenstates (c) $|\psi_1\rangle$ and (d) $|\psi_2\rangle$, (e) and (f) the steady-state intensity patterns as light interacts with the scatterers, and the transmitted states (g) $\hat{t}|\psi_1\rangle$ and (h) $\hat{t}|\psi_2\rangle$.

V. NUMERICAL DEMONSTRATION

We illustrate our theory with a concrete numerical example. Consider a silicon slab waveguide ($n_i = 3.48$) embedded in silica cladding ($n_0 = 1.444$) [Fig. 4(a)]. The waveguide has a thickness of $w = 0.3875$ μm in the x direction and extends along the y and z directions. Light propagates along the z direction with a vacuum wavelength of $\lambda = 1.55$ μm, and the electric field is polarized along the y direction. The waveguide contains four cylindrical scatterers made of lossy silica ($n_s = 1.444 + 0.100i$). The cylinders have diameters of $d_1 = 0.116$ μm, $d_2 = 0.194$ μm, $d_3 = 0.233$ μm, and $d_4 = 0.155$ μm. Their centers are located at $(y_1, z_1) = (-0.80\ \mu\text{m}, 0.097\ \mu\text{m})$, $(y_2, z_2) = (-0.60\ \mu\text{m}, 0.078\ \mu\text{m})$, $(y_3, z_3) = (-0.30\ \mu\text{m}, -0.078\ \mu\text{m})$, and $(y_4, z_4) = (0.10\ \mu\text{m}, -0.097\ \mu\text{m})$, respectively.

We simulate the light propagation in the waveguide using Tidy3D [133], which implements the finite-difference time-domain method. The waveguide supports two eigenmodes, denoted by $|\psi_1\rangle$ and $|\psi_2\rangle$, in its uniform section. Figure 4(b) shows the cross-sectional refractive index profile $n(x)$ of the waveguide and the electric-field profiles of the eigenmodes. We input these eigenmodes from the left side of the scatterers. Figures 4(c) and 4(d) show the intensity distributions of these input eigenmodes. These waves interact with the scatterers and undergo partial transmission, reflection, and absorption [Figs. 4(e) and 4(f)]. We determine the field transmission matrix under the eigenmode

bases

$$G = \begin{pmatrix} 0.146 + 0.394i & 0.484 - 0.471i \\ 0.151 - 0.407i & 0.378 + 0.297i \end{pmatrix}, \tag{42}$$

where the reference planes for incident and transmitted waves are positioned at $z = -4.39$ and 4.00 μm, respectively. From this transmission matrix, we calculate

$$\boldsymbol{\sigma}(G) = \begin{pmatrix} 0.879 \\ 0.528 \end{pmatrix}, \quad \boldsymbol{\sigma}^2(G) = \begin{pmatrix} 0.773 \\ 0.279 \end{pmatrix}, \tag{43}$$

along with the total transmittance vector

$$\boldsymbol{T} = (0.365, 0.687)^{\mathrm{T}} \tag{44}$$

and the direct transmission vector

$$\boldsymbol{t} = (0.146 + 0.394i, 0.378 + 0.297i)^{\mathrm{T}}. \tag{45}$$

Figures 4(g) and 4(h) show the intensity distribution of the transmitted states $\hat{t}|\psi_1\rangle$ and $\hat{t}|\psi_2\rangle$, respectively.

Next we demonstrate unitary control of wave transmission in this system. We place programmable unitary mode converters on each side of the waveguide [Fig. 5(a)]. These converters can take multiple physical forms, such as multiplane light conversion devices and Mach-Zehnder interferometer meshes. The left-hand-side converter transforms each input eigenmode $|\psi_i\rangle$, $i = 1, 2$, into $U|\psi_i\rangle$. This transformed wave then interacts with the scatterers, producing a transmitted state $\hat{t}U|\psi_i\rangle$. The right-hand-side converter further transforms this state into $V^\dagger\hat{t}U|\psi_i\rangle$. By tuning U and V, we control both the total transmittance vector $\boldsymbol{T}[U]$ and the direct transmittance vector $\boldsymbol{t}[U, V]$. Figures 5(b) and 5(c) display the sets of achievable $\{\boldsymbol{T}\}$ and $\{\boldsymbol{t}\}$ under unitary control, showing patterns similar to those in Figs. 2(a) and 3(a). The gray dots mark the values of $\boldsymbol{T}$ and $|\boldsymbol{t}|$ for the original eigenmodes (when $U = V = I$), while the purple dots indicate our target values

$$\boldsymbol{T}_0 = (0.526, 0.526)^{\mathrm{T}}, \quad \boldsymbol{t}_0 = (0.704, 0.704)^{\mathrm{T}}, \tag{46}$$

which achieve unitary uniform total transmittance and direct transmission. Applying Algorithms 2 and 3, we obtain the unitary transformations that achieve the target values

$$U = \begin{pmatrix} -0.938 + 0.000i & 0.346 + 0.000i \\ 0.328 - 0.111i & 0.889 - 0.301i \end{pmatrix}, \tag{47}$$

$$V = \begin{pmatrix} -0.175 - 0.713i & 0.526 - 0.429i \\ -0.159 + 0.660i & 0.718 - 0.152i \end{pmatrix}. \tag{48}$$

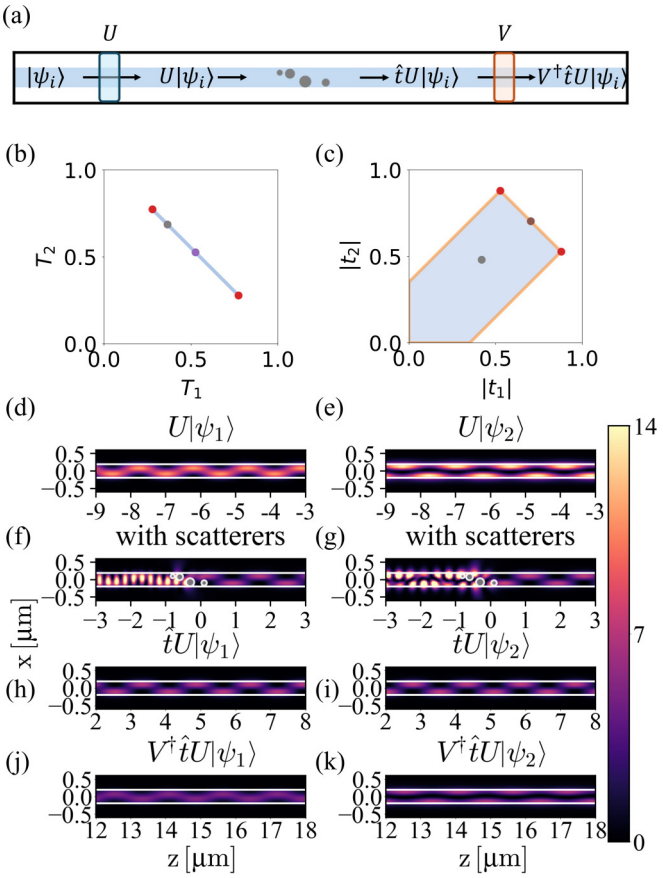

FIG. 5. Unitary control of wave transmission in the waveguide. (a) Schematic showing programmable unitary mode converters U and V added to both sides of the waveguide. The sets of attainable (b) $\{\boldsymbol{T}\}$ and (c) $\{|\boldsymbol{t}|\}$ are under unitary control. Gray dots indicate the values in the absence of unitary control. Purple dots mark the target values achieved via unitary control in Eqs. (47) and (48). Intensity distributions $|E|^2(x, z)$ show the transformed input states (d) $U|\psi_1\rangle$ and (e) $U|\psi_2\rangle$, (f) and (g) the steady-state intensity patterns as light interacts with the scatterers, the immediately transmitted states (h) $\hat{t}U|\psi_1\rangle$ and (i) $\hat{t}U|\psi_2\rangle$, and the final transformed transmitted states (j) $V^\dagger\hat{t}U|\psi_1\rangle$ and (k) $V^\dagger\hat{t}U|\psi_2\rangle$.

Figures 5(d) and 5(e) show the intensity distributions of the transformed input states $U|\psi_1\rangle$ and $U|\psi_2\rangle$. These waves interact with the scatterers, undergoing partial transmission, reflection, and absorption [Figs. 5(f) and 5(g)]. Figures 5(h) and 5(i) display the intensity distributions of the immediately transmitted states $\hat{t}U|\psi_1\rangle$ and $\hat{t}U|\psi_2\rangle$, while Figs. 5(j) and 5(k) show the final transformed transmitted states $V^\dagger\hat{t}U|\psi_1\rangle$ and $V^\dagger\hat{t}U|\psi_2\rangle$. The numerical results demonstrate the implementation of unitary control for manipulating multimode wave transmission.

VI. CONCLUSION

We note several limitations and challenges in the current methodology of unitary control. These challenges naturally

point to promising directions for future research in this field. First, implementing unitary control requires complete knowledge of the transmission matrix, which may not be available in certain applications. Exploring control strategies based on partial transmission matrix information represents an important future direction. Second, our current theory addresses only single-frequency manipulation, and extending it to multifrequency broadband control remains an open challenge. Third, practical deployment requires compact, large-scale, programmable unitary converters. The development of such devices for various practical applications constitutes a technological frontier.

In conclusion, we provided a systematic theory for unitary control of wave transmission. We revealed that singular value inequalities provide the mathematical structure to describe the physics of unitary control. Our results deepen the understanding of unitary control of wave transmission and provide practical guidelines for its implementation.

ACKNOWLEDGMENTS

This work was funded by a Simons Investigator in Physics grant from the Simons Foundation (Grant No. 827065) and by a Multidisciplinary University Research Initiative grant from the U.S. Air Force Office of Scientific Research (Grant No. FA9550-21-1-0312).

APPENDIX A: CHU'S AND FICKUS'S ALGORITHMS

Here we briefly review Chu's [126] and Fickus's [125] algorithms (Algorithms A1 and A2, respectively) for constructing a Hermitian matrix with prescribed diagonal entries and eigenvalues.

ALGORITHM A1. Chu's first algorithm.

One can construct a real symmetric matrix with prescribed eigenvalues $\boldsymbol{\lambda}$ and diagonal entries $\boldsymbol{d}$ by integrating the differential equations

$$\dot{X} = [X, [\mathrm{diag}(X) - \mathrm{diag}(\boldsymbol{d}), X]] \tag{A1}$$

until equilibrium from a starting point $X_0 = Q^{\mathrm{T}}\Lambda Q$, with Q a random orthogonal matrix and $\Lambda = \mathrm{diag}(\boldsymbol{\lambda})$. Here $[A, B] \equiv AB - BA$ is the Lie bracket, $\mathrm{diag}(X)$ is the diagonal matrix with the same diagonal entries of X, and $\mathrm{diag}(\boldsymbol{d})$ is the diagonal matrix with diagonal entries $\boldsymbol{d}$. This algorithm always converges to a valid solution.

ALGORITHM A2. Fickus's algorithm.

One can construct all Hermitian matrices with prescribed eigenvalues $\boldsymbol{\lambda}$ and diagonal entries $\boldsymbol{d}$ using finite frame theory. The explicit steps can be found in Ref. [125].

We also review Chu's algorithm [130] for constructing a matrix with prescribed diagonal entries and singular values.

ALGORITHM A3. Chu's second algorithm.

One can construct a real matrix with prescribed singular values $\boldsymbol{\sigma}$ and diagonal entries $\boldsymbol{d}$ using a recursive method. The explicit codes can be found in Ref. [130].

APPENDIX B: DEMONSTRATION OF ALGORITHM A2

To illustrate Algorithm A2, we consider a 5×5 transmission matrix

$$G = \begin{pmatrix} -0.15 - 0.13i & -0.09 - 0.02i & -0.13 - 0.35i & -0.13 - 0.01i & -0.20 - 0.12i \\ 0.36 - 0.20i & 0.14 + 0.10i & -0.08 - 0.10i & -0.16 + 0.24i & 0.22 - 0.34i \\ 0.44 - 0.14i & -0.11 - 0.05i & -0.07 + 0.22i & -0.04 + 0.15i & -0.19 - 0.19i \\ 0.02 + 0.00i & -0.04 + 0.19i & 0.25 + 0.12i & 0.11 - 0.02i & 0.18 - 0.12i \\ 0.04 - 0.17i & -0.45 - 0.13i & -0.25 - 0.14i & 0.07 - 0.03i & -0.18 - 0.07i \end{pmatrix}, \tag{B1}$$

with

$$\boldsymbol{\sigma}(G) = (0.90, \quad 0.70, \quad 0.50, \quad 0.30, \quad 0.10)^{\mathrm{T}}, \tag{B2}$$

$$\boldsymbol{\sigma}^2(G) = (0.81, \quad 0.49, \quad 0.25, \quad 0.09, \quad 0.01)^{\mathrm{T}}. \tag{B3}$$

The task is to construct a $U[\boldsymbol{T}_0]$, with the randomly assigned goal

$$\boldsymbol{T}_0 = (0.55, \quad 0.20, \quad 0.28, \quad 0.15, \quad 0.46)^{\mathrm{T}}. \tag{B4}$$

First, we check that

$$\boldsymbol{T}_0 \prec \boldsymbol{\sigma}^2(G) \tag{B5}$$

so that $\boldsymbol{T}_0$ is attainable via unitary control. We use Algorithm A2 to obtain

$$U[\boldsymbol{T}_0] = \begin{pmatrix} -0.23+0.00i & 0.53+0.00i & 0.23+0.00i & -0.31+0.00i & 0.72+0.00i \\ 0.10-0.48i & -0.37+0.01i & -0.38-0.09i & -0.62+0.26i & -0.15+0.02i \\ -0.48-0.44i & 0.08-0.04i & -0.35-0.34i & 0.30-0.44i & -0.03+0.19i \\ -0.09-0.17i & 0.35+0.32i & 0.36-0.25i & -0.40+0.00i & 0.58+0.21i \\ -0.32-0.37i & -0.22-0.54i & 0.52+0.32i & -0.05-0.05i & 0.12-0.17i \end{pmatrix}.$$

We verify that

$$\boldsymbol{T}[U] = \boldsymbol{d}(U^\dagger[\boldsymbol{T}_0]G^\dagger GU[\boldsymbol{T}_0]) = \boldsymbol{T}_0. \tag{B6}$$

APPENDIX C: DEMONSTRATION OF ALGORITHM A3

To illustrate Algorithm A3, we consider the same $G \in M_5$ as given in Eq. (B1). The task is to construct a $(U, V)[\boldsymbol{t}_0]$, with the randomly assigned goal

$$\boldsymbol{t}_0 = (0.50, \quad -0.20, \quad 0.10, \quad 0.30, \quad -0.40)^{\mathrm{T}}. \tag{C1}$$

First, we check that

$$|\boldsymbol{t}_0| \prec_w \boldsymbol{\sigma}(G), \quad \sum_{i=1}^{n-1} |\boldsymbol{t}_0|_i^{\downarrow} - |\boldsymbol{t}_0|_n^{\downarrow} \leqslant \sum_{i=1}^{n-1} \boldsymbol{\sigma}_i^{\downarrow}(G) - \boldsymbol{\sigma}_n^{\downarrow}(G) \tag{C2}$$

so that $\boldsymbol{t}_0$ is attainable via unitary control. We use Algorithm A3 to obtain

$$U[\boldsymbol{t}_0] = \begin{pmatrix} 0.27+0.00i & -0.41+0.00i & 0.37+0.00i & -0.52+0.00i & -0.60+0.00i \\ -0.67+0.38i & -0.00+0.22i & -0.23-0.29i & -0.43-0.03i & -0.07+0.17i \\ 0.41-0.03i & -0.14+0.08i & -0.51-0.34i & -0.06-0.60i & 0.02+0.24i \\ 0.20+0.30i & 0.43+0.28i & 0.48-0.19i & -0.37-0.19i & 0.41-0.01i \\ 0.07-0.17i & -0.33-0.62i & 0.30+0.02i & -0.05-0.03i & 0.48+0.39i \end{pmatrix}.$$

$$V[\boldsymbol{t}_0] = \begin{pmatrix} -0.19-0.43i & 0.25-0.38i & -0.60+0.35i & 0.14+0.21i & -0.05+0.16i \\ -0.43-0.34i & -0.02-0.14i & 0.19-0.08i & -0.70+0.07i & -0.05-0.37i \\ 0.20+0.17i & -0.13+0.07i & -0.15+0.15i & -0.39+0.39i & 0.72+0.22i \\ 0.18-0.23i & -0.24+0.61i & -0.03+0.51i & -0.21+0.10i & -0.40+0.11i \\ 0.49-0.28i & -0.26-0.51i & 0.41-0.06i & -0.02+0.29i & -0.20+0.24i \end{pmatrix}.$$

We verify that

$$\boldsymbol{t}[U, V] = \boldsymbol{d}(V^\dagger[\boldsymbol{t}_0]GU[\boldsymbol{t}_0]) = \boldsymbol{t}_0. \tag{C3}$$

APPENDIX D: PROOF OF EQ. (41)

To prove Eq. (41), we consider the whole scattering matrix of the medium

$$S = \begin{pmatrix} R_1 & \tilde{G} \\ G & R_2 \end{pmatrix} \in M_{2n}, \tag{D1}$$

where R_1 and R_2 are the reflection matrices on the left and right sides, respectively. If the system is reciprocal, then [132]

$$S = S^{\mathrm{T}}, \tag{D2}$$

which implies that

$$\tilde{G} = G^{\mathrm{T}}, \tag{D3}$$

and thus

$$\boldsymbol{\sigma}(\tilde{G}) = \boldsymbol{\sigma}(G). \tag{D4}$$

If the system is energy conserving, then [132]

$$S^\dagger S = SS^\dagger = I_{2n}. \tag{D5}$$

From $S^\dagger S = I_{2n}$ we obtain

$$R_1^\dagger R_1 + G^\dagger G = I_n. \tag{D6}$$

From $SS^\dagger = I_{2n}$ we obtain

$$R_1 R_1^\dagger + \tilde{G}\tilde{G}^\dagger = I_n. \tag{D7}$$

Therefore,

$$\boldsymbol{\sigma}^2(G) = \boldsymbol{\lambda}(G^\dagger G) = \boldsymbol{\lambda}(I_n - R_1^\dagger R_1) = \mathbf{1} - \boldsymbol{\sigma}^2(R_1), \tag{D8}$$

$$\boldsymbol{\sigma}^2(\tilde{G}) = \boldsymbol{\lambda}(\tilde{G}\tilde{G}^\dagger) = \boldsymbol{\lambda}(I_n - R_1 R_1^\dagger) = \mathbf{1} - \boldsymbol{\sigma}^2(R_1). \tag{D9}$$

Thus,

$$\boldsymbol{\sigma}(\tilde{G}) = \boldsymbol{\sigma}(G). \tag{D10}$$

This completes the proof of Eq. (41).

[1] *Waves and Imaging through Complex Media*, edited by P. Sebbah (Kluwer Academic, Dordrecht, 2001).

[2] V. Ntziachristos, Going deeper than microscopy: The optical imaging frontier in biology, Nat. Methods **7**, 603 (2010).

[3] T. Čižmár and K. Dholakia, Exploiting multimode waveguides for pure fibre-based imaging, Nat. Commun. **3**, 1027 (2012).

[4] S. Kang, S. Jeong, W. Choi, H. Ko, T. D. Yang, J. H. Joo, J.-S. Lee, Y.-S. Lim, Q.-H. Park, and W. Choi, Imaging deep within a scattering medium using collective accumulation of single-scattered waves, Nat. Photonics **9**, 253 (2015).

[5] C. Guo, M. Xiao, M. Minkov, Y. Shi, and S. Fan, Photonic crystal slab Laplace operator for image differentiation, Optica **5**, 251 (2018).

[6] C. Guo, M. Xiao, M. Minkov, Y. Shi, and S. Fan, Isotropic wavevector domain image filters by a photonic crystal slab device, J. Opt. Soc. Am. A **35**, 1685 (2018).

[7] S. Yoon, M. Kim, M. Jang, Y. Choi, W. Choi, S. Kang, and W. Choi, Deep optical imaging within complex scattering media, Nat. Rev. Phys. **2**, 141 (2020).

[8] H. Wang, C. Guo, Z. Zhao, and S. Fan, Compact incoherent image differentiation with nanophotonic structures, ACS Photonics **7**, 338 (2020).

[9] O. Y. Long, C. Guo, H. Wang, and S. Fan, Isotropic topological second-order spatial differentiator operating in transmission mode, Opt. Lett. **46**, 3247 (2021).

[10] J. Bertolotti and O. Katz, Imaging in complex media, Nat. Phys. **18**, 1008 (2022).

[11] H. Wang, W. Jin, C. Guo, N. Zhao, S. P. Rodrigues, and S. Fan, Design of compact meta-crystal slab for general optical convolution, ACS Photonics **9**, 1358 (2022).

[12] O. Y. Long, C. Guo, W. Jin, and S. Fan, Polarization-independent isotropic nonlocal metasurfaces with wavelength-controlled functionality, Phys. Rev. Appl. **17**, 024029 (2022).

[13] D. A. B. Miller, Establishing optimal wave communication channels automatically, J. Lightwave Technol. **31**, 3987 (2013).

[14] D. A. B. Miller, Waves, modes, communications, and optics: A tutorial, Adv. Opt. Photonics **11**, 679 (2019).

[15] S. SeyedinNavadeh, M. Milanizadeh, F. Zanetto, G. Ferrari, M. Sampietro, M. Sorel, D. A. B. Miller, A. Melloni, and F. Morichetti, Determining the optimal communication channels of arbitrary optical systems using integrated photonic processors, Nat. Photonics **18**, 149 (2024).

[16] J. Aulbach, B. Gjonaj, P. M. Johnson, A. P. Mosk, and A. Lagendijk, Control of light transmission through opaque scattering media in space and time, Phys. Rev. Lett. **106**, 103901 (2011).

[17] R. Sarma, A. Yamilov, S. F. Liew, M. Guy, and H. Cao, Control of mesoscopic transport by modifying transmission channels in opaque media, Phys. Rev. B **92**, 214206 (2015).

[18] M. Mounaix, D. Andreoli, H. Defienne, G. Volpe, O. Katz, S. Grésillon, and S. Gigan, Spatiotemporal coherent control of light through a multiple scattering medium with the multispectral transmission matrix, Phys. Rev. Lett. **116**, 253901 (2016).

[19] S. Jeong, Y.-R. Lee, W. Choi, S. Kang, J. H. Hong, J.-S. Park, Y.-S. Lim, H.-G. Park, and W. Choi, Focusing of light energy inside a scattering medium by controlling the time-gated multiple light scattering, Nat. Photonics **12**, 277 (2018).

[20] T. Liu and A. Fiore, Designing open channels in random scattering media for on-chip spectrometers, Optica **7**, 934 (2020).

[21] A. Turpin, I. Vishniakou, and J. D. Seelig, Light scattering control in transmission and reflection with neural networks, Opt. Express **26**, 30911 (2018).

[22] S. Leedumrongwatthanakun, L. Innocenti, H. Defienne, T. Juffmann, A. Ferraro, M. Paternostro, and S. Gigan, Programmable linear quantum networks with a multimode fibre, Nat. Photonics **14**, 139 (2020).

[23] G. Wetzstein, A. Ozcan, S. Gigan, S. Fan, D. Englund, M. Soljačić, C. Denz, D. A. B. Miller, and D. Psaltis, Inference in artificial intelligence with deep optics and photonics, Nature (London) **588**, 39 (2020).

[24] H. Wang, C. Guo, W. Jin, A. Y. Song, and S. Fan, Engineering arbitrarily oriented spatiotemporal optical vortices using transmission nodal lines, Optica **8**, 966 (2021).

[25] C. Guo, M. Xiao, M. Orenstein, and S. Fan, Structured 3D linear space– time light bullets by nonlocal nanophotonics, Light Sci. Appl. **10**, 160 (2021).

[26] Y. Shen, Q. Zhan, L. G. Wright, D. N. Christodoulides, F. Wise, A. Willner, K. Zou, Z. Zhao, M. A. Porras, A. Chong, C. Wan, K. Y. Bliokh, C.-T. Liao, C. Hernandez Garcia, M. M. Murnane, M. Yessenov, A. Abouraddy, L. J. Wong, M. Go, S. Kumar *et al.*, Roadmap on spatiotemporal light fields, J. Opt. **25**, 093001 (2023).

[27] Y. Guan, O. Katz, E. Small, J. Zhou, and Y. Silberberg, Polarization control of multiply scattered light through random media by wavefront shaping, Opt. Lett. **37**, 4663 (2012).

[28] O. Katz, E. Small, and Y. Silberberg, Looking around corners and through thin turbid layers in real time with scattered incoherent light, Nat. Photonics **6**, 549 (2012).

[29] R. Horstmeyer, H. Ruan, and C. Yang, Guidestar-assisted wavefront-shaping methods for focusing light into biological tissue, Nat. Photonics **9**, 563 (2015).

[30] I. M. Vellekoop, Feedback-based wavefront shaping, Opt. Express **23**, 12189 (2015).

[31] H. Yu, J. Park, K. Lee, J. Yoon, K. Kim, S. Lee, and Y. Park, Recent advances in wavefront shaping techniques for biomedical applications, Curr. Appl. Phys. **15**, 632 (2015).

[32] P. Pai, J. Bosch, M. Kühmayer, S. Rotter, and A. P. Mosk, Scattering invariant modes of light in complex media, Nat. Photonics **15**, 431 (2021).

[33] S. Rotter and S. Gigan, Light fields in complex media: Mesoscopic scattering meets wave control, Rev. Mod. Phys. **89**, 015005 (2017).

[34] H. Cao, A. P. Mosk, and S. Rotter, Shaping the propagation of light in complex media, Nat. Phys. **18**, 994 (2022).

[35] Z. Yaqoob, D. Psaltis, M. S. Feld, and C. Yang, Optical phase conjugation for turbidity suppression in biological samples, Nat. Photonics **2**, 110 (2008).

[36] S. Fan and J. M. Kahn, Principal modes in multimode waveguides, Opt. Lett. **30**, 135 (2005).

[37] T. Čižmár and K. Dholakia, Shaping the light transmission through a multimode optical fibre: Complex transformation analysis and applications in biophotonics, Opt. Express **19**, 18871 (2011).

[38] I. N. Papadopoulos, S. Farahi, C. Moser, and D. Psaltis, Focusing and scanning light through a multimode optical fiber using digital phase conjugation, Opt. Express **20**, 10583 (2012).

[39] J. Carpenter, B. J. Eggleton, and J. Schröder, Observation of Eisenbud–Wigner–Smith states as principal modes in multimode fibre, Nat. Photonics **9**, 751 (2015).

[40] W. Xiong, P. Ambichl, Y. Bromberg, B. Redding, S. Rotter, and H. Cao, Spatiotemporal control of light transmission through a multimode fiber with strong mode coupling, Phys. Rev. Lett. **117**, 053901 (2016).

[41] G. Lerosey, J. De Rosny, A. Tourin, and M. Fink, Focusing beyond the diffraction limit with far-field time reversal, Science **315**, 1120 (2007).

[42] I. Vellekoop and A. Mosk, Phase control algorithms for focusing light through turbid media, Opt. Commun. **281**, 3071 (2008).

[43] O. Katz, E. Small, Y. Bromberg, and Y. Silberberg, Focusing and compression of ultrashort pulses through scattering media, Nat. Photonics **5**, 372 (2011).

[44] D. J. McCabe, A. Tajalli, D. R. Austin, P. Bondareff, I. A. Walmsley, S. Gigan, and B. Chatel, Spatio-temporal focusing of an ultrafast pulse through a multiply scattering medium, Nat. Commun. **2**, 447 (2011).

[45] X. Xu, H. Liu, and L. V. Wang, Time-reversed ultrasonically encoded optical focusing into scattering media, Nat. Photonics **5**, 154 (2011).

[46] J.-H. Park, C. Park, H. Yu, J. Park, S. Han, J. Shin, S. H. Ko, K. T. Nam, Y.-H. Cho, and Y. Park, Subwavelength light focusing using random nanoparticles, Nat. Photonics **7**, 454 (2013).

[47] B. Blochet, L. Bourdieu, and S. Gigan, Focusing light through dynamical samples using fast continuous wavefront optimization, Opt. Lett. **42**, 4994 (2017).

[48] I. M. Vellekoop and A. P. Mosk, Universal optimal transmission of light through disordered materials, Phys. Rev. Lett. **101**, 120601 (2008).

[49] S. M. Popoff, G. Lerosey, R. Carminati, M. Fink, A. C. Boccara, and S. Gigan, Measuring the transmission matrix in optics: An approach to the study and control of light propagation in disordered media, Phys. Rev. Lett. **104**, 100601 (2010).

[50] M. Kim, Y. Choi, C. Yoon, W. Choi, J. Kim, Q.-H. Park, and W. Choi, Maximal energy transport through disordered media with the implementation of transmission eigenchannels, Nat. Photonics **6**, 581 (2012).

[51] Z. Shi and A. Z. Genack, Transmission eigenvalues and the bare conductance in the crossover to Anderson localization, Phys. Rev. Lett. **108**, 043901 (2012).

[52] H. Yu, T. R. Hillman, W. Choi, J. O. Lee, M. S. Feld, R. R. Dasari, and Y. K. Park, Measuring large optical transmission matrices of disordered media, Phys. Rev. Lett. **111**, 153902 (2013).

[53] B. Gérardin, J. Laurent, A. Derode, C. Prada, and A. Aubry, Full transmission and reflection of waves propagating through a maze of disorder, Phys. Rev. Lett. **113**, 173901 (2014).

[54] A. Peña, A. Girschik, F. Libisch, S. Rotter, and A. A. Chabanov, The single-channel regime of transport through random media, Nat. Commun. **5**, 3488 (2014).

[55] S. M. Popoff, A. Goetschy, S. F. Liew, A. D. Stone, and H. Cao, Coherent control of total transmission of light through disordered media, Phys. Rev. Lett. **112**, 133903 (2014).

[56] M. Davy, Z. Shi, J. Wang, X. Cheng, and A. Z. Genack, Transmission eigenchannels and the densities of states of random media, Phys. Rev. Lett. **114**, 033901 (2015).

[57] Z. Shi, M. Davy, and A. Z. Genack, Statistics and control of waves in disordered media, Opt. Express **23**, 12293 (2015).

[58] N. Bender, A. Yamilov, H. Yılmaz, and H. Cao, Fluctuations and correlations of transmission eigenchannels in diffusive media, Phys. Rev. Lett. **125**, 165901 (2020).

[59] T. Čižmár, M. Mazilu, and K. Dholakia, *In situ* wavefront correction and its application to micromanipulation, Nat. Photonics **4**, 388 (2010).

[60] C. Gonzalez-Ballestero, M. Aspelmeyer, L. Novotny, R. Quidant, and O. Romero-Isart, Levitodynamics: Levitation and control of microscopic objects in vacuum, Science **374**, eabg3027 (2021).

[61] J. Hüpfl, N. Bachelard, M. Kaczvinszki, M. Horodynski, M. Kühmayer, and S. Rotter, Optimal cooling of multiple levitated particles through far-field wavefront shaping, Phys. Rev. Lett. **130**, 083203 (2023).

[62] I. M. Vellekoop and A. P. Mosk, Focusing coherent light through opaque strongly scattering media, Opt. Lett. **32**, 2309 (2007).

[63] H. Yu, K. Lee, and Y. Park, Ultrahigh enhancement of light focusing through disordered media controlled by mega-pixel modes, Opt. Express **25**, 8036 (2017).

[64] S. F. Liew, S. M. Popoff, S. W. Sheehan, A. Goetschy, C. A. Schmuttenmaer, A. D. Stone, and H. Cao, Coherent control of photocurrent in a strongly scattering photoelectrochemical system, ACS Photonics **3**, 449 (2016).

[65] C. Guo and S. Fan, Topological winding guaranteed coherent orthogonal scattering, Phys. Rev. A **109**, L061503 (2024).

[66] S. Berdagué and P. Facq, Mode division multiplexing in optical fibers, Appl. Opt. **21**, 1950 (1982).

[67] L.-W. Luo, N. Ophir, C. P. Chen, L. H. Gabrielli, C. B. Poitras, K. Bergmen, and M. Lipson, WDM-compatible mode-division multiplexing on a silicon chip, Nat. Commun. **5**, 3069 (2014).

[68] Y. Su, Y. He, H. Chen, X. Li, and G. Li, Perspective on mode-division multiplexing, Appl. Phys. Lett. **118**, 200502 (2021).

[69] M. Reck, A. Zeilinger, H. J. Bernstein, and P. Bertani, Experimental realization of any discrete unitary operator, Phys. Rev. Lett. **73**, 58 (1994).

[70] D. A. B. Miller, Self-aligning universal beam coupler, Opt. Express **21**, 6360 (2013).

[71] D. A. B. Miller, Self-configuring universal linear optical component [Invited], Photonics Res. **1**, 1 (2013).

[72] J. Carolan, C. Harrold, C. Sparrow, E. Martín-López, N. J. Russell, J. W. Silverstone, P. J. Shadbolt, N. Matsuda, M. Oguma, M. Itoh, G. D. Marshall, M. G. Thompson, J. C. F. Matthews, T. Hashimoto, J. L. O'Brien, and A. Laing, Universal linear optics, Science **349**, 711 (2015).

[73] D. A. B. Miller, Perfect optics with imperfect components, Optica **2**, 747 (2015).

[74] W. R. Clements, P. C. Humphreys, B. J. Metcalf, W. S. Kolthammer, and I. A. Walmsley, Optimal design for universal multiport interferometers, Optica **3**, 1460 (2016).

[75] A. Ribeiro, A. Ruocco, L. Vanacker, and W. Bogaerts, Demonstration of a 4×4-port universal linear circuit, Optica **3**, 1348 (2016).

[76] C. M. Wilkes, X. Qiang, J. Wang, R. Santagati, S. Paesani, X. Zhou, D. A. B. Miller, G. D. Marshall, M. G. Thompson, and J. L. O'Brien, 60 dB high-extinction auto-configured Mach–Zehnder interferometer, Opt. Lett. **41**, 5318 (2016).

[77] A. Annoni, E. Guglielmi, M. Carminati, G. Ferrari, M. Sampietro, D. A. B. Miller, A. Melloni, and F. Morichetti, Unscrambling light—automatically undoing strong mixing between modes, Light Sci. Appl. **6**, e17110 (2017).

[78] D. A. B. Miller, Setting up meshes of interferometers – reversed local light interference method, Opt. Express **25**, 29233 (2017).

[79] D. Perez, I. Gasulla, F. J. Fraile, L. Crudgington, D. J. Thomson, A. Z. Khokhar, K. Li, W. Cao, G. Z. Mashanovich, and J. Capmany, Silicon photonics rectangular universal interferometer, Laser Photonics Rev. **11**, 1700219 (2017).

[80] N. C. Harris, J. Carolan, D. Bunandar, M. Prabhu, M. Hochberg, T. Baehr-Jones, M. L. Fanto, A. M. Smith, C. C. Tison, P. M. Alsing, and D. Englund, Linear programmable nanophotonic processors, Optica **5**, 1623 (2018).

[81] S. Pai, B. Bartlett, O. Solgaard, and D. A. B. Miller, Matrix optimization on universal unitary photonic devices, Phys. Rev. Appl. **11**, 064044 (2019).

[82] J.-F. Morizur, L. Nicholls, P. Jian, S. Armstrong, N. Treps, B. Hage, M. Hsu, W. Bowen, J. Janousek, and H.-A. Bachor, Programmable unitary spatial mode manipulation, J. Opt. Soc. Am. A **27**, 2524 (2010).

[83] G. Labroille, B. Denolle, P. Jian, P. Genevaux, N. Treps, and J.-F. Morizur, Efficient and mode selective spatial mode multiplexer based on multi-plane light conversion, Opt. Express **22**, 15599 (2014).

[84] R. Tanomura, Y. Taguchi, R. Tang, T. Tanemura, and Y. Nakano, *Proceedings of the 2022 Conference on Lasers and Electro-Optics Pacific Rim* (Optica, Washington, DC, 2022), paper CWP13A_02.

[85] H. Kupianskyi, S. A. R. Horsley, and D. B. Phillips, High-dimensional spatial mode sorting and optical circuit design using multi-plane light conversion, APL Photonics **8**, 026101 (2023).

[86] Y. Taguchi, Y. Wang, R. Tanomura, T. Tanemura, and Y. Ozeki, Iterative configuration of programmable unitary converter based on few-layer redundant multiplane light conversion, Phys. Rev. Appl. **19**, 054002 (2023).

[87] Y. Zhang and N. K. Fontaine, Multi-Plane Light Conversion: A Practical Tutorial, arXiv:2304.11323.

[88] J. Carolan, M. Mohseni, J. P. Olson, M. Prabhu, C. Chen, D. Bunandar, M. Y. Niu, N. C. Harris, F. N. C. Wong, M. Hochberg, S. Lloyd, and D. Englund, Variational quantum unsampling on a quantum photonic processor, Nat. Phys. **16**, 322 (2020).

[89] A. W. Elshaari, W. Pernice, K. Srinivasan, O. Benson, and V. Zwiller, Hybrid integrated quantum photonic circuits, Nat. Photonics **14**, 285 (2020).

[90] J. Wang, F. Sciarrino, A. Laing, and M. G. Thompson, Integrated photonic quantum technologies, Nat. Photonics **14**, 273 (2020).

[91] Y. Chi, J. Huang, Z. Zhang, J. Mao, Z. Zhou, X. Chen, C. Zhai, J. Bao, T. Dai, H. Yuan, M. Zhang, D. Dai, B. Tang, Y. Yang, Z. Li, Y. Ding, L. K. Oxenløwe, M. G. Thompson, J. L. O'Brien, Y. Li *et al.*, A programmable qudit-based quantum processor, Nat. Commun. **13**, 1166 (2022).

[92] L. S. Madsen, F. Laudenbach, M. F. Askarani, F. Rortais, T. Vincent, J. F. F. Bulmer, F. M. Miatto, L. Neuhaus, L. G. Helt, M. J. Collins, A. E. Lita, T. Gerrits, S. W. Nam, V. D. Vaidya, M. Menotti, I. Dhand, Z. Vernon, N. Quesada, and J. Lavoie, Quantum computational advantage with a programmable photonic processor, Nature (London) **606**, 75 (2022).

[93] E. Pelucchi, G. Fagas, I. Aharonovich, D. Englund, E. Figueroa, Q. Gong, H. Hannes, J. Liu, C.-Y. Lu, N. Matsuda, J.-W. Pan, F. Schreck, F. Sciarrino, C. Silberhorn, J. Wang, and K. D. Jöns, The potential and global outlook of integrated photonics for quantum technologies, Nat. Rev. Phys. **4**, 194 (2022).

[94] Y. Shen, N. C. Harris, S. Skirlo, M. Prabhu, T. Baehr-Jones, M. Hochberg, X. Sun, S. Zhao, H. Larochelle, D. Englund, and M. Soljačić, Deep learning with coherent nanophotonic circuits, Nat. Photonics **11**, 441 (2017).

[95] M. Prabhu, C. Roques-Carmes, Y. Shen, N. Harris, L. Jing, J. Carolan, R. Hamerly, T. Baehr-Jones, M. Hochberg, V. Čeperić, J. D. Joannopoulos, D. R. Englund, and M. Soljačić, Accelerating recurrent Ising machines in photonic integrated circuits, Optica **7**, 551 (2020).

[96] H. Zhang, M. Gu, X. D. Jiang, J. Thompson, H. Cai, S. Paesani, R. Santagati, A. Laing, Y. Zhang, M. H. Yung, Y. Z. Shi, F. K. Muhammad, G. Q. Lo, X. S. Luo, B. Dong, D. L. Kwong, L. C. Kwek, and A. Q. Liu, An optical neural chip for implementing complex-valued neural network, Nat. Commun. **12**, 457 (2021).

[97] F. Ashtiani, A. J. Geers, and F. Aflatouni, An on-chip photonic deep neural network for image classification, Nature (London) **606**, 501 (2022).

[98] S. Bandyopadhyay, A. Sludds, S. Krastanov, R. Hamerly, N. Harris, D. Bunandar, M. Streshinsky, M. Hochberg, and D. Englund, Single chip photonic deep neural network with accelerated training, Nat. Photon. **18**, 1335 (2024).

[99] S. Ohno, R. Tang, K. Toprasertpong, S. Takagi, and M. Takenaka, Si microring resonator crossbar array for on-chip inference and training of the optical neural network, ACS Photonics **9**, 2614 (2022).

[100] Z. Chen, A. Sludds, R. Davis III, I. Christen, L. Bernstein, L. Ateshian, T. Heuser, N. Heermeier, J. A. Lott, S. Reitzenstein, R. Hamerly, and D. Englund, Deep learning with coherent VCSEL neural networks, Nat. Photonics **17**, 723 (2023).

[101] S. Pai, Z. Sun, T. W. Hughes, T. Park, B. Bartlett, I. A. D. Williamson, M. Minkov, M. Milanizadeh, N. Abebe, F. Morichetti, A. Melloni, S. Fan, O. Solgaard, and D. A. B. Miller, Experimentally realized in situ backpropagation for deep learning in photonic neural networks, Science **380**, 398 (2023).

[102] R. Burgwal, W. R. Clements, D. H. Smith, J. C. Gates, W. S. Kolthammer, J. J. Renema, and I. A. Walmsley, Using an imperfect photonic network to implement random unitaries, Opt. Express **25**, 28236 (2017).

[103] D. Melati, A. Alippi, A. Annoni, N. Peserico, and A. Melloni, Integrated all-optical MIMO demultiplexer for mode- and wavelength-division-multiplexed transmission, Opt. Lett. **42**, 342 (2017).

[104] K. Choutagunta, I. Roberts, D. A. B. Miller, and J. M. Kahn, Adapting Mach–Zehnder mesh equalizers in direct-detection

mode-division-multiplexed links, J. Lightwave Technol. **38**, 723 (2020).
[105] S. Buddhiraju, A. Dutt, M. Minkov, I. A. D. Williamson, and S. Fan, Arbitrary linear transformations for photons in the frequency synthetic dimension, Nat. Commun. **12**, 2401 (2021).
[106] C. Guo and S. Fan, Majorization theory for unitary control of optical absorption and emission, Phys. Rev. Lett. **130**, 146202 (2023).
[107] C. Guo and S. Fan, Unitary control of partially coherent waves. I. Absorption, Phys. Rev. B **110**, 035430 (2024).
[108] C. Guo and S. Fan, Unitary control of partially coherent waves. II. Transmission or reflection, Phys. Rev. B **110**, 035431 (2024).
[109] C. Guo, D. A. B. Miller, and S. Fan, Transport measurements of majorization order for wave coherence, arXiv:2408.06386.
[110] D. A. B. Miller, Communicating with waves between volumes: Evaluating orthogonal spatial channels and limits on coupling strengths, Appl. Opt. **39**, 1681 (2000).
[111] D. A. B. Miller, All linear optical devices are mode converters, Opt. Express **20**, 23985 (2012).
[112] Y. Yue, Y. Yan, N. Ahmed, J.-Y. Yang, L. Zhang, Y. Ren, H. Huang, K. M. Birnbaum, B. I. Erkmen, S. Dolinar, M. Tur, and A. E. Willner, Mode properties and propagation effects of optical orbital angular momentum (OAM) modes in a ring fiber, IEEE Photonics J. **4**, 535 (2012).
[113] N. Bozinovic, Y. Yue, Y. Ren, M. Tur, P. Kristensen, H. Huang, A. E. Willner, and S. Ramachandran, Terabit-scale orbital angular momentum mode division multiplexing in fibers, Science **340**, 1545 (2013).
[114] D. J. Richardson, J. M. Fini, and L. E. Nelson, Space-division multiplexing in optical fibres, Nat. Photonics **7**, 354 (2013).
[115] C. Brunet, P. Vaity, Y. Messaddeq, S. LaRochelle, and L. A. Rusch, Design, fabrication and validation of an OAM fiber supporting 36 states, Opt. Express **22**, 26117 (2014).
[116] Y. Lian, Y. Yu, S. Han, N. Luan, Y. Wang, and Z. Lu, OAM beams generation technology in optical fiber: A review, IEEE Sens. J. **22**, 3828 (2022).
[117] C. Guo, J. Li, M. Xiao, and S. Fan, Singular topology of scattering matrices, Phys. Rev. B **108**, 155418 (2023).
[118] A. W. Marshall, I. Olkin, and B. C. Arnold, *Inequalities: Theory of Majorization and Its Applications*, 2nd ed. (Springer Science+Business Media, New York, 2011).
[119] Y. V. Nazarov, Weak localization and the transmission matrix, Phys. Rev. B **52**, 4720 (1995).
[120] R. A. Horn and C. R. Johnson, *Matrix Analysis*, 2nd ed. (Cambridge University Press, Cambridge, 2012).
[121] C. Guo and S. Fan, Passivity constraints on the relations between transmission, reflection, and absorption eigenvalues, Phys. Rev. B **110**, 205431 (2024).
[122] I. Schur, Uber eine klasse von mittelbildungen mit anwendungen auf die determinantentheorie, Sitzungsber. Berliner Math. Ges. **22**, 51 (1923).
[123] A. Horn, Doubly stochastic matrices and the diagonal of a rotation matrix, Am. J. Math. **76**, 620 (1954).
[124] R. Rado, An inequality, J. London Math. Soc. **s1-27**, 1 (1952).
[125] M. Fickus, D. G. Mixon, M. J. Poteet, and N. Strawn, Constructing all self-adjoint matrices with prescribed spectrum and diagonal, Adv. Comput. Math. **39**, 585 (2013).
[126] M. T. Chu, Constructing a Hermitian matrix from its diagonal entries and eigenvalues, SIAM J. Matrix Anal. Appl. **16**, 207 (1995).
[127] F.-Y. Sing, Some results on matrices with prescribed diagonal elements and singular values, Can. Math. Bull. **19**, 89 (1976).
[128] R. C. Thompson, Singular values, diagonal elements, and convexity, SIAM J. Appl. Math. **32**, 39 (1977).
[129] C. Guo and S. Fan, Reciprocity constraints on reflection, Phys. Rev. Lett. **128**, 256101 (2022).
[130] M. T. Chu, On constructing matrices with prescribed singular values and diagonal elements, Linear Algebra Appl. **288**, 11 (1999).
[131] Z. Zhao, C. Guo, and S. Fan, Connection of temporal coupled-mode-theory formalisms for a resonant optical system and its time-reversal conjugate, Phys. Rev. A **99**, 033839 (2019).
[132] C. Guo, Z. Zhao, and S. Fan, Internal transformations and internal symmetries in linear photonic systems, Phys. Rev. A **105**, 023509 (2022).
[133] T. W. Hughes, M. Minkov, V. Liu, Z. Yu, and S. Fan, A perspective on the pathway toward full wave simulation of large area metalenses, Appl. Phys. Lett. **119**, 150502 (2021).